Nonlinear development of matrix converter instabilities

Stephen M. Cox (stephen.cox@nottingham.ac.uk)
School of Mathematical Sciences, University of Nottingham, University Park, Nottingham NG7 2RD, United Kingdom

Jon C. Clare (jon.clare@nottingham.ac.uk)
School of Electrical and Electronic Engineering, University of Nottingham, University Park, Nottingham NG7 2RD, United Kingdom

Abstract.
Matrix converters convert a three-phase alternating-current power supply to a power supply of a different peak voltage and frequency, and are an emerging technology in a wide variety of applications. However, they are susceptible to an instability, whose behaviour is examined herein. The desired "steady-state" mode of operation of the matrix converter becomes unstable in a Hopf bifurcation as the output/input voltage transfer ratio, q, is increased through some threshold value, q_c. Through weakly nonlinear analysis and direct numerical simulation of an averaged model, we show that this bifurcation is *subcritical* for typical parameter values, leading to hysteresis in the transition to the oscillatory state: there may thus be undesirable large-amplitude oscillations in the output voltages even when q is below the linear stability threshold value q_c.

Keywords: power electronics, matrix converter, instability

1. Introduction

The matrix converter is an important emerging technology for the conversion of one alternating-current (AC) power supply into another AC power supply, with different voltage and frequency [1]. The three input lines to the matrix converter provide a three-phase power supply (i.e. they each have a sinusoidally varying voltage, but with a phase difference of one-third of a cycle between any two input lines). The desired output of the matrix converter is similarly a three-phase power supply.

The matrix converter works by connecting each output line to the various input lines in succession, according to some switching protocol, at high frequency, in an attempt to synthesise the desired outputs. Filters suppress the high-frequency components of the output. A significant advantage of the matrix converter over other technologies is that it requires no bulky intermediate storage elements, thus making it particularly suitable for applications such as aerospace, where space and weight are at a premium.

Unfortunately, the matrix converter can become unstable; as a consequence the intended "steady-state" output is spoilt by large-amplitude, high-frequency ripple. This new "oscillatory state" is highly undesirable in applications; its origin and nonlinear development are analysed in this paper. The key parameter is the output/input voltage transfer ratio, q. A linear stability analysis of the steady-state output indicates that the ripple appears through a Hopf bifurcation as q is increased through some threshold value q_c; the value of q_c and other results such as the ripple frequency at onset have been computed by Casadei et al. [2, 3] for some typical system parameter values. Here we extend analysis of the behaviour of the matrix converter to the nonlinear regime. (Prior investigation of the nonlinear development of the instability has so far been based on an approximation to the oscillatory state [2]; a comparison of our results with those from this approximation are discussed below, in Section 3.5.2.)

Most of our analysis assumes that the switching protocol is decided *instantaneously*, based upon a knowledge of the present state of the inputs and the desired outputs. However, an important feature of real matrix converters is that their operation is digital: the input is sampled, and the appropriate switching protocol is then calculated (by a microprocessor) in order to achieve the relevant outputs. There is thus a delay between the sampling of the inputs and the implementation of the corresponding switching protocol, while the necessary calculations are performed. We briefly describe in the analysis below a model for this so-called transport delay (although our analysis primarily concerns the idealised limit of zero delay).

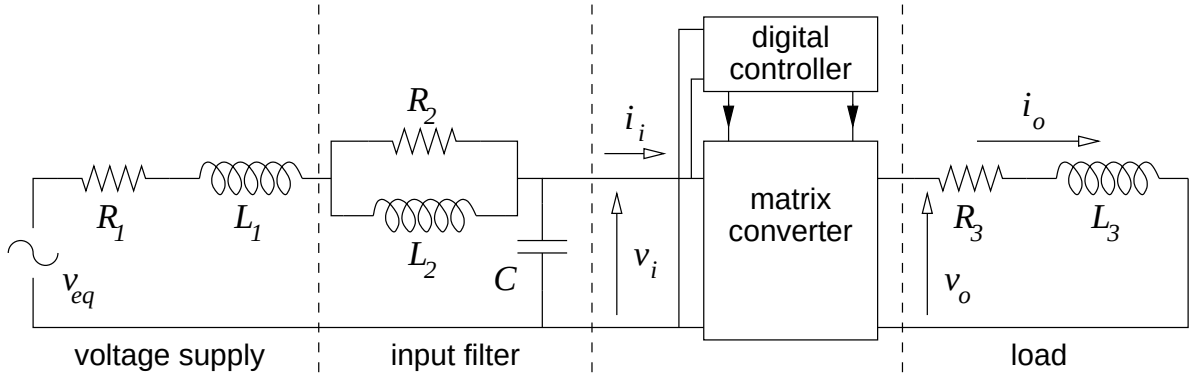

Figure 1. Schematic of the matrix converter circuit modelled here.

Our mathematical model involves averaging over the high-frequency switching, and neglects any effects due to the switching action itself. Thus our analysis of the stability of the matrix converter is limited to so-called "slow-scale" instabilities [4, 5, 6, 7], which involve time scales much longer than the switching period. While it is possible that the matrix converter has in addition "fast-scale" instabilities [4, 5, 6, 7], which arise on time scales comparable with the switching period, we are unable to examine those here, in the averaged model. We return to the question of the validity of the averaging procedure at the end of this paper.

In Section 2 we set out the mathematical model [2, 3] that we use to investigate the behaviour of the matrix converter, and indicate the means by which we solve the governing equations. In Section 3 we treat the case of zero transport delay, which allows significant analytical progress in calculating both the steady-state and oscillatory outputs. The latter are calculated both by a weakly nonlinear analysis close to the onset of the oscillatory solutions, and by directly solving the governing nonlinear equations numerically. The case of nonzero transport delay is treated briefly in Section 4. We show the results of some numerical simulations using the Saber package in Section 5, and our conclusions are summarised in Section 6.

2. Mathematical formulation

Our development of a mathematical formulation of the stability problem follows that of Casadei et al. [2] and [3]. We begin by noting that the matrix converter works by switching each output between the three input lines at high frequency (for example, typically switching at 12.5kHz; this is significantly greater than the input and output frequencies, which are of the order of 10–100Hz). The outputs therefore contain significant high-frequency contributions [8]. However, in applications these high-frequency contributions are filtered out, and it is the low-frequency contributions which approximate the intended sinusoidal outputs. To render the problem tractable, we shall follow Casadei et al. in ignoring high-frequency contributions to the input and output spectra in this stability calculation. We shall see later that we need to re-examine this fundamental modelling approximation, but for the moment we simply adopt it, and pursue the consequences. Thus in our formulation of the stability problem, the effects of the switching are ignored. A schematic of the circuit considered is given in Figure 1.

In order to describe the behaviour of the converter in a concise notational framework, we use the concept of a space vector [9]. To explain this concept, we begin by noting that there are three input and three output lines for the matrix converter. The three power supply voltages (of which one is indicated explicitly in Figure 1) may be written

$$v_{eq}^{(1)}(t) = V_{eq}\cos\omega_i t, \qquad v_{eq}^{(2)}(t) = V_{eq}\cos(\omega_i t + 2\pi/3), \qquad v_{eq}^{(3)}(t) = V_{eq}\cos(\omega_i t + 4\pi/3), \qquad (1)$$

where we have denoted the peak input voltage by V_{eq} and the input (angular) frequency by ω_i. Any two of the input lines are thus out of phase by one-third of a cycle. We now choose to describe all three (real-valued) power supply voltages using the single complex quantity (the space vector)

$$v_{eq}(t) \equiv \tfrac{2}{3}(v_{eq}^{(1)}(t) + v_{eq}^{(2)}(t)\mathrm{e}^{-2\pi\mathrm{i}/3} + v_{eq}^{(3)}(t)\mathrm{e}^{2\pi\mathrm{i}/3}). \tag{2}$$

In view of the constraint

$$v_{eq}^{(1)}(t) + v_{eq}^{(2)}(t) + v_{eq}^{(3)}(t) = 0, \tag{3}$$

which follows from (1), the physical power supply voltages may all be recovered from the space vector $v_{eq}(t)$ using

$$v_{eq}^{(1)}(t) = \Re(v_{eq}(t)), \qquad v_{eq}^{(2)}(t) = \Re(v_{eq}(t)\mathrm{e}^{2\pi\mathrm{i}/3}), \qquad v_{eq}^{(3)}(t) = \Re(v_{eq}(t)\mathrm{e}^{-2\pi\mathrm{i}/3}),$$

where $\Re$ denotes the real part. From (1) and (2), it follows that the space vector for the power supply is thus simply

$$v_{eq}(t) = V_{eq}\mathrm{e}^{\mathrm{i}\omega_i t}.$$

Similarly, given the currents $i_o^{(1)}(t)$, $i_o^{(2)}(t)$ and $i_o^{(3)}(t)$, and voltages $v_o^{(1)}(t)$, $v_o^{(2)}(t)$ and $v_o^{(3)}(t)$ in the three output lines, we define the corresponding output current and voltage space vectors to be

$$i_o(t) \equiv \tfrac{2}{3}(i_o^{(1)}(t) + i_o^{(2)}(t)\mathrm{e}^{-2\pi\mathrm{i}/3} + i_o^{(3)}(t)\mathrm{e}^{2\pi\mathrm{i}/3})$$

and

$$v_o(t) \equiv \tfrac{2}{3}(v_o^{(1)}(t) + v_o^{(2)}(t)\mathrm{e}^{-2\pi\mathrm{i}/3} + v_o^{(3)}(t)\mathrm{e}^{2\pi\mathrm{i}/3}).$$

From this point, where we refer to input or output currents or voltages, we shall mean the corresponding space vector, unless stated otherwise.

Losses in the power supply and the input filter have the consequence that the voltage delivered to the matrix converter is not precisely $v_{eq}(t)$. A specification of the actual input voltage to the converter is most readily described in the frequency domain, so that

$$\hat{v}_{eq}(\omega) = Z_i(\omega)\hat{i}_i(\omega) + \hat{v}_i(\omega), \tag{4}$$

where $\hat{}$ denotes the Fourier transform. Here $Z_i(\omega)$ is the effective input impedance, which for the circuit shown in Figure 1 is

$$Z_i(\omega) = \frac{R_1R_2 + (R_1L_2 + R_2L_1 + R_2L_2)\mathrm{i}\omega - L_1L_2\omega^2}{R_2 + (R_1R_2C + L_2)\mathrm{i}\omega - (R_1L_2 + R_2L_1 + R_2L_2)C\omega^2 - L_1L_2C\mathrm{i}\omega^3}.$$

Given the series resistive–inductive load indicated in Figure 1, the output currents and voltages from the matrix converter are related by

$$\hat{v}_o(\omega) = Z_o(\omega)\hat{i}_o(\omega), \tag{5}$$

where Z_o is the output impedance

$$Z_o(\omega) = R_3 + L_3\mathrm{i}\omega.$$

The switching in the matrix converter is carried out at a frequency much higher than either the input or the desired output, and we simplify our analysis of the device by considering only the low-frequency components of the inputs and outputs. Thus, rather than consider the details of the switchings, we need to know only the corresponding duty cycles, in other words the proportions of each switching period during which each output line is connected to each input line. The relationships between the input and output sides of the matrix converter are then compactly given by

$$v_o(t) = \tfrac{3}{2}\left(m_i^*(t)v_i(t) + m_d(t)v_i^*(t)\right), \tag{6}$$

$$i_i(t) = \tfrac{3}{2}\left(m_i(t)i_o(t) + m_d(t)i_o^*(t)\right), \tag{7}$$

where $i_i(t)$ denotes the input current, the asterisk denotes complex conjugation and $m_d(t)$ and $m_i(t)$ are the relevant duty cycle space vectors [9]. The latter quantities are computed using the input voltages to the matrix converter and the intended (or "reference") output voltage, whose space vector is

$$v_{or}(t) = V_{or}\mathrm{e}^{\mathrm{i}\omega_o t},$$

ω_o being the intended output (angular) frequency. It is important to note that, because of the processing time required to compute $m_d(t)$ and $m_i(t)$, the duty cycles that are applied are in general delayed versions of the corresponding "reference" values $m_{dr}(t)$ and $m_{ir}(t)$, which are calculated [9] according to

$$m_{dr}(t) = \frac{v_{or}(t)}{3v_i^*(t)}, \tag{8}$$

$$m_{ir}(t) = \frac{v_{or}^*(t)}{3v_i^*(t)}. \tag{9}$$

We begin our analysis with the case of zero delay, in which case

$$m_d(t) = m_{dr}(t), \tag{10}$$

$$m_i(t) = m_{ir}(t), \tag{11}$$

and substitution of (8) and (9) in (6) leads to the result $v_o(t) = v_{or}(t)$, so that the output voltage is exactly equal to the desired output reference voltage. (In the presence of delays, as we shall consider in Section 4, however, (10) and (11) are modified, and the actual output $v_o(t)$ is distorted slightly from the intended $v_{or}(t)$.)

The mathematical problem governing the behaviour of the matrix converter is thus given by the eight equations (4)–(11) for the eight unknown quantities v_i, i_i, v_o, i_o, m_d, m_i, m_{dr} and m_{ir}. The problem is greatly simplified if we factor out the underlying oscillations of input and output quantities (i.e. if we move into rotating frames for the space vectors) and write the unknowns in the form

$$v_i(t) = \mathrm{e}^{\mathrm{i}\omega_i t}g_i(t), \qquad i_i(t) = \mathrm{e}^{\mathrm{i}\omega_i t}f_i(t), \qquad v_o(t) = \mathrm{e}^{\mathrm{i}\omega_o t}g_o(t), \qquad i_o(t) = \mathrm{e}^{\mathrm{i}\omega_o t}f_o(t), \tag{12}$$

and

$$m_d(t) = \mathrm{e}^{\mathrm{i}(\omega_i+\omega_o)t}h_d(t), \qquad m_i(t) = \mathrm{e}^{\mathrm{i}(\omega_i-\omega_o)t}h_i(t), \tag{13}$$

$$m_{dr}(t) = \mathrm{e}^{\mathrm{i}(\omega_i+\omega_o)t}h_{dr}(t), \qquad m_{ir}(t) = \mathrm{e}^{\mathrm{i}(\omega_i-\omega_o)t}h_{ir}(t). \tag{14}$$

Then the unknowns are

$$f_i(t), \quad g_i(t), \quad f_o(t), \quad g_o(t), \quad h_d(t), \quad h_i(t), \quad h_{dr}(t) \quad \text{and} \quad h_{ir}(t). \tag{15}$$

2.1. Behaviour of the matrix converter

The desired, steady-state operating conditions of the matrix converter correspond to constant values of the variables (15). For general delays, it is a messy calculation to determine even this steady-state solution, but in the special case of zero delay, the problem simplifies considerably – see [2] and [3]. We find that the steady-state solution changes little as a function of the delay time, for reasonable values of this parameter: the reason for this insensitivity is that the delay is on the order of the switching period, which is much less than the periods of the inputs and outputs. This insensitivity provides some prima facie reassurance that our neglect of explicit switching effects is a reasonable modelling step.

Below we shall examine the stability of the steady-state solution to infinitesimal disturbances, according to (4)–(11). We shall find that the steady-state solution becomes unstable to "oscillatory" solutions, in which the variables (15) oscillate in time-periodic fashion, with some period $2\pi/\omega_r$, where $\omega_r \gg \omega_i, \omega_o$.

For infinitesimal oscillations, the value of ω_r arises from the linear stability analysis. However, the value of ω_r for finite-amplitude oscillations varies as a function of the amplitude of the oscillatory state; we explicitly consider this variation below, in a weakly nonlinear analysis for oscillations of small (but finite) amplitude. To be consistent in neglecting switching effects, we require that $\omega_r \ll \omega_s$, where ω_s is the (angular) switching frequency.

To calculate the oscillatory solutions numerically, we apply a spectral method, and write $f_i(t)$ in the form

$$f_i(t) = \sum_{n=-\infty}^{\infty} f_i^n \mathrm{e}^{n\mathrm{i}\omega_r t}, \tag{16}$$

with similar Fourier series for the other variables in (15). Of the eight governing equations (4)–(11), the four that are *linear* may be used to determine $g_i(t)$, $f_o(t)$, $h_d(t)$ and $h_i(t)$ in terms of the remaining unknowns, through

$$g_i^n = -Z_i(\omega_i + n\omega_r) f_i^n + V_{eq}\delta_{n0}, \tag{17}$$
$$f_o^n = g_o^n / Z_o(\omega_o + n\omega_r), \tag{18}$$
$$h_d^n = h_{dr}^n, \tag{19}$$
$$h_i^n = h_{ir}^n, \tag{20}$$

for $n = 0, \pm1, \pm2, \ldots$, where δ represents the Kronecker-δ, so that $\delta_{n0} = 1$ if $n = 0$, but $\delta_{n0} = 0$ otherwise. There then remain four sets of *nonlinear* equations to solve, for the unknowns g_o^n, f_i^n, h_{dr}^n and h_{ir}^n, which may be written

$$g_o^n = \tfrac{3}{2} \sum_{p=-\infty}^{\infty} \left(h_i^{p-n\,*} g_i^p + h_d^{n-p} g_i^{-p\,*} \right), \tag{21}$$

$$f_i^n = \tfrac{3}{2} \sum_{p=-\infty}^{\infty} \left(h_i^{n-p} f_o^p + h_d^{n-p} f_o^{-p\,*} \right), \tag{22}$$

$$\sum_{p=-\infty}^{\infty} g_i^{p-n\,*} h_{dr}^p = \tfrac{1}{3} V_{or} \delta_{n0}, \tag{23}$$

$$\sum_{p=-\infty}^{\infty} g_i^{p-n\,*} h_{ir}^p = \tfrac{1}{3} V_{or}^* \delta_{n0}, \tag{24}$$

for $n = 0, \pm1, \pm2, \ldots$.

For numerical purposes all sums in expressions like (16) are truncated at $n = \pm N$ for some sufficiently large value of N; the governing nonlinear equations (21)–(24) are also considered only for $-N \le n \le N$. These governing equations are further simplified by choosing the phase of the outputs so that V_{or} is real-valued (which may straightforwardly be done by an appropriate choice of the time origin); then

$$h_{ir}^n = h_{dr}^n$$

for all n, so the number of unknowns is reduced, which significantly speeds up the numerics.

It is crucial to note that the problem (21)–(24) for the oscillatory state has a time translation symmetry, which reflects the arbitrariness of the phase of the oscillations: correspondingly, we may replace t by $t + \tau$, for any constant τ in expressions such as (16). This time translation symmetry is equivalent to transforming the Fourier coefficients according to $f_i^n \mapsto f_i^n \mathrm{e}^{n\mathrm{i}\omega_r\tau}$, with corresponding expressions for the other variables. Thus we may arbitrarily choose the argument of one of the Fourier coefficients (for $n \neq 0$). This degree of freedom means that equations (21)–(24) are sufficient to determine not only the various Fourier mode amplitudes *up to rotations corresponding to the time translation symmetry*, but also the oscillation frequency ω_r. To fix the Fourier mode amplitudes in the numerical results that follow, we choose to set

$$\Im(g_i^1) = 0, \tag{25}$$

where $\Im$ denotes the imaginary part, although we emphasise that this choice is necessary only to fix the phase of the oscillations, and does not affect any of the diagnostics presented below.

3. Results for zero delay

Before (briefly) considering the general problem later, we first treat the special case when there is zero delay between computation and implementation of the duty cycles (the fast-processor limit). Then the problem simplifies considerably. We note from (6), (8), (9), (10), (11), (12), (13) and (14) that the output voltage is precisely the output reference voltage, i.e.

$$g_o = V_{or}.$$

We next describe a calculation of the steady-state solution and an analysis of its stability to infinitesimal perturbations. We then compute small-amplitude, weakly nonlinear oscillatory solutions, and finally present numerical results for finite-amplitude oscillatory solutions.

3.1. Steady-state solution

We now derive expressions for the steady-state solution with zero delay (little corresponding detail is given in [2, 3], and it is useful for some later analysis to record details here). Since $g_o = V_{or}$ in this case, it follows from (18) that

$$f_o = \frac{V_{or}}{Z_o(\omega_o)} = \frac{V_{or}}{R_3 + L_3 \mathrm{i}\omega_o}. \tag{26}$$

Thus the output power, which in the space vector representation is $P_o \equiv \frac{3}{2}\Re(g_o^* f_o)$, may be written [2]

$$P_o = \tfrac{3}{2}|V_{or}|^2 \Re(Y_o(\omega_o)), \tag{27}$$

where $Y_o(\omega_o) \equiv 1/Z_o(\omega_o)$ is the output admittance. We observe that P_o is independent of time in this zero-delay case, even when the solution itself for (15) is oscillatory (this is not so when delays are present). But P_o is also the *input* power, because in the present model we ignore losses in the matrix converter, and this observation allows to derive a useful relationship between the input voltage and current. To do so, we first note that the most common mode of operation of the matrix converter [2] has a modulation strategy in which the input current and voltage vectors are kept in phase; then the input current and voltage satisfy [2]

$$g_{is}^* f_{is} = \tfrac{2}{3} P_o, \tag{28}$$

where the additional subscript s denotes the value of the relevant quantity in the steady-state solution.

From (7), (8), (9) and (26), the input current satisfies

$$f_i(t) = \tfrac{3}{2}\left(h_i(t) f_o(t) + h_d(t) f_o^*(t)\right) = \frac{|V_{or}|^2 \Re(Y_o(\omega_o))}{g_i^*(t)} \tag{29}$$

and, from (4), we are left with the single equation

$$V_{eq} = \frac{Q}{g_{is}^*} + g_{is} \tag{30}$$

from which to determine the steady-state solution, where

$$Q = Z_i(\omega_i)|V_{or}|^2 \Re(Y_o(\omega_o)). \tag{31}$$

To solve (30), we first multiply each side by its complex conjugate to give

$$|V_{eq}|^2 = \frac{|Q|^2}{|g_{is}|^2} + 2\Re(Q) + |g_{is}|^2. \tag{32}$$

Table I. System parameters for power supply, input filter and output load (taken from [3]).

supply	filter	load
$R_1 = 0.55\Omega$	$R_2 = 300\Omega$	$R_3 = 8.2\Omega$
$L_1 = 0.90$mH	$L_2 = 1.16$mH	$L_3 = 1.3$mH
$V_{eq} = 110\sqrt{2}$V	$C = 4.5\mu$F	$\omega_o = 2\pi \times 100$rad/s
$\omega_i = 2\pi \times 50$rad/s		

This may be viewed as a quadratic equation for $|g_{is}|^2$, which has solutions provided

$$(2\Re(Q) - |V_{eq}|^2)^2 - 4|Q|^2 \geq 0,$$

or, equivalently, provided

$$|V_{eq}|^4 - 4\Re(Q)|V_{eq}|^2 - 4\Im(Q)^2 \geq 0. \tag{33}$$

If we fix the input and output impedances and the output reference voltage (so that Q is fixed), then this condition may be interpreted as saying that the input voltage must be sufficient to deliver the intended output.

Supposing (33) to be satisfied, then there are in general *two* solutions to (32), given by

$$|g_{is}|^2 = \tfrac{1}{2}|V_{eq}|^2 - \Re(Q) \pm \left[(\tfrac{1}{2}|V_{eq}|^2 - \Re(Q))^2 - |Q|^2\right]^{1/2}. \tag{34}$$

Only one of these solutions corresponds to the expected normal operating conditions for the steady state; the other is not of physical relevance. The different nature of the two mathematical solutions of the steady-state problem is made clear if we examine the limit in which $V_{or} \to 0$, so that $Q \to 0$; then the two solutions are given by

$$|g_{is}^+|^2 \sim |V_{eq}|^2, \qquad |g_{is}^-|^2 \sim \frac{|Q|^2}{|V_{eq}|^2},$$

where we have denoted the solutions corresponding to the positive or negative square root in (34) in the obvious way. Since g_{is} represents the input voltage to the matrix converter and V_{eq} represents the power supply voltage, it is clear that in the limit of small demand output voltage these two should agree. The physically relevant steady-state solution is thus given by taking the *positive* square root in (34), so that

$$|g_{is}|^2 = \tfrac{1}{2}|V_{eq}|^2 - \Re(Q) + \left[(\tfrac{1}{2}|V_{eq}|^2 - \Re(Q))^2 - |Q|^2\right]^{1/2}. \tag{35}$$

However, this expression provides only the modulus; the value of g_{is} itself is obtained from (30), which yields

$$g_{is} = \frac{V_{eq}|g_{is}|^2}{|g_{is}|^2 + Q}, \tag{36}$$

where $|g_{is}|^2$ is known from (35).

Table I shows some typical values, taken from [3], for the supply, filter and load parameters; these values are adopted for the remainder of this paper (these parameter values differ from those used in [2]). Note that V_{eq} is chosen so that the rms input voltages are 110V; the input and output frequencies are 50Hz and 100Hz, respectively. For these values, we show in Figure 2 the corresponding values of $|g_{is}|$ for the two steady-state solutions as a function of V_{or}. We see that, for the physically meaningful steady-state solution, the actual input voltage to the matrix converter varies little over a wide range of reference output voltages.

Having computed the steady-state solution, we next examine its stability to infinitesimal perturbations.

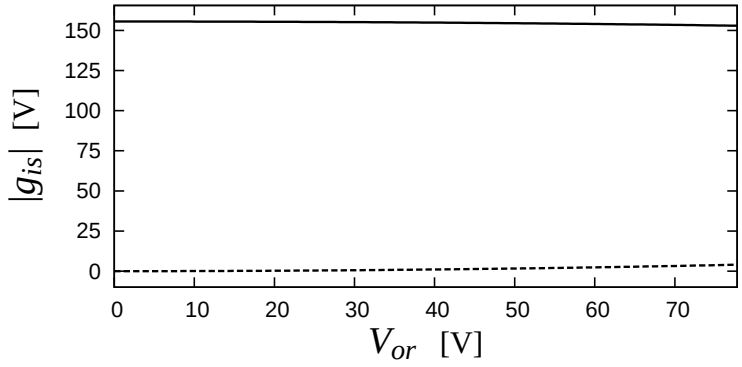

Figure 2. Plot of the two solutions to (34) as a function of the reference output voltage V_{or}. Only the upper solution is physically relevant.

3.2. Linear stability of the steady-state solution

In order to examine the linear stability of the steady-state solution found above, it is useful to formulate the nonlinear ordinary differential equation governing the behaviour of the matrix converter, in the present zero-delay case (our approach is thus rather different from that of Casadei et al. [2, 3]). We proceed by introducing the differential operators

$$\mathcal{X}(f(t);\omega) = R_1R_2f(t) + (R_1L_2 + R_2L_1 + R_2L_2)\left(\mathrm{i}\omega + \frac{\mathrm{d}}{\mathrm{d}t}\right)f(t) + L_1L_2\left(\mathrm{i}\omega + \frac{\mathrm{d}}{\mathrm{d}t}\right)^2 f(t)$$

and

$$\begin{aligned}\mathcal{Y}(f(t);\omega) \;=\; & R_2f(t) + (R_1R_2C + L_2)\left(\mathrm{i}\omega + \frac{\mathrm{d}}{\mathrm{d}t}\right)f(t) \\ & + (R_1L_2 + R_2L_1 + R_2L_2)C\left(\mathrm{i}\omega + \frac{\mathrm{d}}{\mathrm{d}t}\right)^2 f(t) + L_1L_2C\left(\mathrm{i}\omega + \frac{\mathrm{d}}{\mathrm{d}t}\right)^3 f(t).\end{aligned}$$

Then with the input current and voltage vectors in phase, so that

$$g_i^* f_i = \tfrac{2}{3}P_o \tag{37}$$

(and we recall that the power P_o is constant), (4) is equivalent to the ordinary differential equation

$$\mathcal{X}(\tfrac{2}{3}P_o/g_i^*(t);\omega_i) + \mathcal{Y}(g_i(t);\omega_i) = \mathcal{Y}(1;\omega_i)V_{eq}. \tag{38}$$

To determine the stability of the steady-state solution, we consider the evolution of infinitesimal perturbations to the steady-state solution $g_i = g_{is}$ of (38). We thus write

$$g_i(t) = g_{is} + \epsilon g_{i1}(t),$$

where $\epsilon \ll 1$, and consider the linearised version of (38) which results from neglecting terms of $O(\epsilon^2)$ and smaller. Thus

$$-\frac{2P_o}{3g_{is}^{*2}}\mathcal{X}(g_{i1}^*(t);\omega_i) + \mathcal{Y}(g_{i1}(t);\omega_i) = 0. \tag{39}$$

(A corresponding calculation in the Fourier frequency domain is described by Casadei et al. [3].) The stability of the steady-state solution $g_i = g_{is}$ may now be ascertained by considering disturbances of the form

$$g_{i1}(t) = \mathrm{e}^{\lambda t} + a\mathrm{e}^{\lambda^* t}. \tag{40}$$

Substitution of this ansatz in (39) then yields

$$-\frac{2P_o}{3g_{is}^{*2}}\mathcal{X}(\mathrm{e}^{\lambda^* t};\omega_i) + a\mathcal{Y}(\mathrm{e}^{\lambda^* t};\omega_i) - \frac{2P_o}{3g_{is}^{*2}}a^*\mathcal{X}(\mathrm{e}^{\lambda t};\omega_i) + \mathcal{Y}(\mathrm{e}^{\lambda t};\omega_i) = 0.$$

Since the terms on the left-hand side of this equation in $\mathrm{e}^{\lambda t}$ and $\mathrm{e}^{\lambda^* t}$ must independently vanish, it follows that

$$a = \frac{2P_o\mathcal{X}(\mathrm{e}^{\lambda^* t};\omega_i)}{3g_{is}^{*2}\mathcal{Y}(\mathrm{e}^{\lambda^* t};\omega_i)}, \qquad a^* = \frac{3g_{is}^{*2}\mathcal{Y}(\mathrm{e}^{\lambda t};\omega_i)}{2P_o\mathcal{X}(\mathrm{e}^{\lambda t};\omega_i)}. \tag{41}$$

By taking the complex conjugate of the first of these, we obtain two expressions for a^*. Then using the result that $\mathcal{X}(\mathrm{e}^{\lambda^* t};\omega_i)$ is the complex conjugate of $\mathcal{X}(\mathrm{e}^{\lambda t};-\omega_i)$, which is readily obtained from the definition of the operator $\mathcal{X}$, and equating the two resulting expressions for a^*, we see that the eigenvalue λ satisfies

$$\mathcal{Y}(\mathrm{e}^{\lambda t};\omega_i)\mathcal{Y}(\mathrm{e}^{\lambda t};-\omega_i) = \frac{4P_o^2}{9|g_{is}|^4}\mathcal{X}(\mathrm{e}^{\lambda t};\omega_i)\mathcal{X}(\mathrm{e}^{\lambda t};-\omega_i), \tag{42}$$

and the constant a is given by the first of (41).

In practice, the eigenvalue problem (42) must be solved numerically. In doing so, we find that the physically meaningful steady-state solution is stable (all eigenvalues have negative real part) for $V_{or} < V_{or,c}$, where

$$V_{or,c} \approx 26.88.$$

The steady-state solution becomes unstable at $V_{or} = V_{or,c}$, at which point the real part of a complex-conjugate pair of eigenvalues becomes positive; hence this is a Hopf bifurcation. At the bifurcation, the relevant eigenvalues are given by $\lambda = \pm\mathrm{i}\omega_r$, where $\omega_r \approx 10373.5$ (hence the oscillation frequency is approximately 1651Hz). Furthermore, at the bifurcation point, the steady-state solution has $|g_{is}| = 155.3$, and hence the critical value of the output-to-input transfer ratio

$$q \equiv \left|\frac{V_{or}}{g_i}\right|$$

is $q_c \approx 0.173$. Below this threshold, the steady-state solution is linearly stable; above, it is unstable.

3.3. Weakly nonlinear oscillatory solution

We now extend the linear stability analysis of the previous section to derive weakly nonlinear expressions for the output near the onset of the instability. In this analysis, we use the output power P_o as our bifurcation parameter, although we could equally well carry out an equivalent calculation using V_{or} (or q) as the bifurcation parameter. We consider values of P_o close to threshold, so that

$$P_o = P_0 + \epsilon^2 P_2,$$

where $P_2 = O(1)$, and again $\epsilon \ll 1$ is a small parameter. Correspondingly, we expand the input voltage function as

$$g_i(t) = g_{is} + \epsilon g_{i1}(t) + \epsilon^2 g_{i2}(t) + \epsilon^3 g_{i3}(t) + \cdots,$$

and substitute both expansions in (38). A consideration of terms at successive powers of ϵ in (38) then leads to a weakly nonlinear description of the solution near the onset of the instability.

At $O(\epsilon^0)$ we recover the problem for the steady state, whose solution is given by (35) and (36).

At $O(\epsilon^1)$ we recover the linear stability problem (39). The linear stability threshold described in the previous section corresponds to

$$P_0 = \tfrac{3}{2}|V_{or,c}|^2\Re(Y_o(\omega_o)) \approx 130.84,$$

where we have used (27) to relate the output power and the reference output voltage. Furthermore, we see, from (40), that $g_{i1}(t)$ takes the form

$$g_{i1}(t) = A(\mathrm{e}^{\mathrm{i}\omega t} + a\mathrm{e}^{-\mathrm{i}\omega t}),$$

where A is an amplitude which will be determined later in the calculation, and

$$a = \frac{2P_0\mathcal{X}(1;\omega_i-\omega_r)}{3g_{is}^{*2}\mathcal{Y}(1;\omega_i-\omega_r)} = \frac{3g_{is}^2\mathcal{Y}^*(1;\omega_i+\omega_r)}{2P_0\mathcal{X}^*(1;\omega_i+\omega_r)} \approx 0.6013 - 0.7589\mathrm{i}.$$

We take the amplitude A to be a real number; this restriction is always possible, provided we choose the time origin appropriately for the oscillations. Here the angular frequency

$$\omega = \omega_r + \epsilon^2\omega_2 \tag{43}$$

of the oscillations is equal to the critical value ω_r, plus a small correction $\epsilon^2\omega_2$ due to the finite amplitude of the solution; this correction will be determined later in the calculation.

At $O(\epsilon^2)$ the equation (38) contains forcing terms of the form $\mathrm{e}^{\pm 2\mathrm{i}\omega t}$ and time-independent terms. The solution is found to be

$$g_{i2}(t) = G_2A^2\mathrm{e}^{2\mathrm{i}\omega t} + G_0 + G_{-2}A^2\mathrm{e}^{-2\mathrm{i}\omega t},$$

where the coefficients are

$$\begin{aligned} G_2 &\approx -0.000556 - 0.000144\mathrm{i}, \\ G_0 &\approx (0.0000142 - 0.0000752\mathrm{i})A^2 - (0.00716 + 0.00832\mathrm{i})P_2 \\ G_{-2} &\approx -0.0000269 - 0.000713\mathrm{i}. \end{aligned}$$

At $O(\epsilon^3)$ in (38) we find that $g_{i3}(t)$ satisfies

$$\begin{aligned} -\frac{2P_0}{3g_{is}^{*2}}\mathcal{X}(g_{i3}^*(t);\omega_i) + \mathcal{Y}(g_{i3}(t);\omega_i) &= \frac{2P_0}{3g_{is}^{*4}}\mathcal{X}(g_{i1}^{*3}(t);\omega_i) - \frac{4P_0}{3g_{is}^{*3}}\mathcal{X}(g_{i1}^*(t)g_{i2}^*(t);\omega_i) \\ &\quad + \frac{2P_2}{3g_{is}^{*2}}\mathcal{X}(g_{i1}^*(t);\omega_i) + \frac{2P_o\omega_2}{3g_{is}^{*2}}\mathcal{X}_2 - \omega_2\mathcal{Y}_2. \end{aligned} \tag{44}$$

Here $\mathcal{X}_2$ and $\mathcal{Y}_2$ represent the corrections to the linear operators $\mathcal{X}$ and $\mathcal{Y}$ arising from the oscillations in $g_{i1}(t)$ having angular frequency ω rather than ω_r. More precisely,

$$\begin{aligned} \mathcal{X}(g_{i1}^*(t);\omega_i) &= \mathcal{X}(\mathrm{e}^{-\mathrm{i}\omega_r t} + a^*\mathrm{e}^{\mathrm{i}\omega_r t};\omega_i) + \epsilon^2\omega_2\mathcal{X}_2 + \cdots, \\ \mathcal{Y}(g_{i1}(t);\omega_i) &= \mathcal{Y}(\mathrm{e}^{\mathrm{i}\omega_r t} + a\mathrm{e}^{-\mathrm{i}\omega_r t};\omega_i) + \epsilon^2\omega_2\mathcal{Y}_2 + \cdots, \end{aligned}$$

where ω is given by (43). The right-hand side of (44) comprises terms of the form $\mathrm{e}^{\pm\mathrm{i}\omega t}$ and $\mathrm{e}^{\pm 3\mathrm{i}\omega t}$; the former terms are resonant, and a nonsecular solution for $g_{i3}(t)$ is possible only if a solvability condition is satisfied by the resonant forcing terms. This solvability condition is readily determined: if we denote the resonant terms on the right-hand side of (44) by

$$C\mathrm{e}^{\mathrm{i}\omega t} + D^*\mathrm{e}^{-\mathrm{i}\omega t}.$$

then C and D must satisfy

$$\frac{2P_0}{3g_{is}^2}\mathcal{X}(1;\omega_r-\omega_i)C + \mathcal{Y}(1;\omega_r+\omega_i)D = 0.$$

This solvability condition provides (from real and imaginary parts) both the frequency correction and an expression for the amplitude A in terms of P_2: we find

$$\omega_2 = 0.1721P_2, \qquad A^2 \approx -102.4P_2. \tag{45}$$

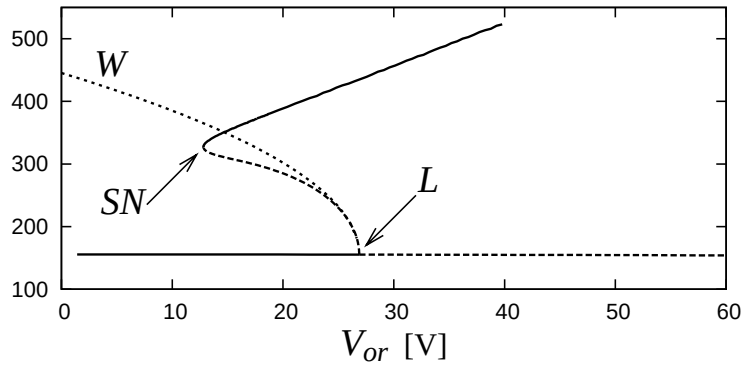

Figure 3. Solutions to the ODE problem (38) as a function of the output reference voltage V_{or}. The nearly horizontal line represents the steady-state solution and the other curve represents the oscillatory solution. Plotted vertically is, for the steady state, $\Re(g_i)$, and for the oscillatory solution the maximum value of $\Re(g_i(t))$ over the cycle (both in Volts). Stable solutions are represented by a solid line and unstable by a dashed line. The point at which the steady state becomes linearly unstable is marked "L" and the saddle–node point is marked "SN". The oscillatory branch terminates when the numerical procedure requires too many Fourier modes to continue. The curve marked "W" gives results from the weakly nonlinear analysis of Section 3.3.

The important result here is that, in view of the expression for A^2 in (45), this weakly nonlinear solution exists only when $P_2 < 0$, in other words when the output power P_o is *less than* the threshold P_0 for instability of the steady-state solution (equivalently, when $V_{or} < V_{or,c}$): the bifurcation is *subcritical*. We discuss the consequences of the subcritical nature of the Hopf bifurcation after first extending these weakly nonlinear solutions to a fully nonlinear numerical solution.

3.4. Fully nonlinear oscillatory solution

To go further than the linear stability calculation of the steady state and the weakly nonlinear calculation of the previous section, we have used two independent methods to find the fully nonlinear oscillatory solutions numerically. First we have used AUTO, which is a continuation and bifurcation package for ordinary differential equations that is ideally suited to tracking the solutions of (38). Then as a check we have solved the nonlinear system (21)–(24) of algebraic equations for the Fourier coefficients; more specifically, we have solved numerically the coupled equations

$$g_i^n = -Z_i(\omega_i + n\omega_r) f_i^n + V_{eq}\delta_{n0}, \qquad n = -N, \ldots, N \tag{46}$$

and

$$\sum_{p=-N}^{N} g_i^{p*} f_i^p = \tfrac{2}{3} P_o, \tag{47}$$

together with (25), where P_o is given by (27).

Results from the two methods agree, provided enough Fourier modes are retained in (46) and (47) ($N = 11$ seems ample near the onset of the oscillatory state; we need to take N around 75 to get good convergence on the upper part of the solution branch). Solutions obtained from the Fourier-series method are shown in Figure 3 for the parameter values in Table I. The linear stability picture of the steady-state solution described above is confirmed, as is the weakly nonlinear calculation of the oscillatory state: a quantitative comparison is shown in Figure 3 between numerics and the weakly nonlinear solution. In particular, the numerics confirms the weakly nonlinear prediction that the oscillatory solution bifurcates *subcritically*, that is, it branches into the region $V < V_{or,c}$. The oscillatory solutions are thus unstable near their birth in the Hopf bifurcation. However, they become stable in a saddle–node bifurcation at

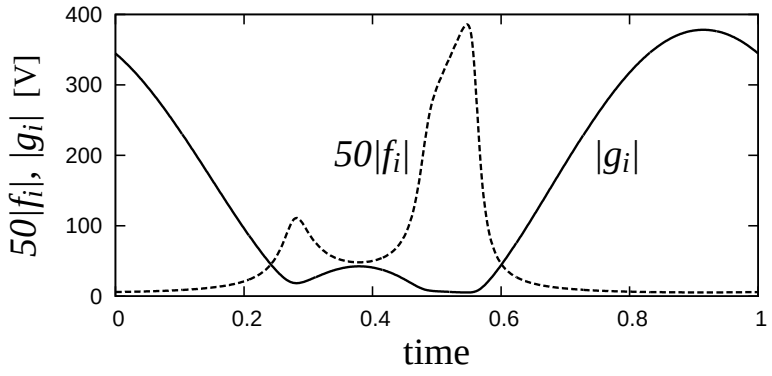

Figure 4. Solution to the ODE problem (38) for $V_{or} = 18.38$ (on the upper, stable branch of solutions). Plot of $50|f_i(t)|$ (dashed line) and $|g_i(t)|$ (solid line). In each case, for plotting purposes, the period has been normalised to 1.

$V_{or} = V_{or,sn}$, where

$$V_{or,sn} \approx 12.82.$$

These weakly nonlinear and fully nonlinear results are practically significant because they indicate that the threshold value $V_{or,c}$, calculated on the basis of a linearisation around the steady-state solution [2, 3], does not represent the smallest value of V_{or} for which oscillatory solutions exist. In fact, the oscillatory states exist down to $V_{or} = V_{or,sn}$, which is less than 50% of the linear stability threshold voltage $V_{or,c}$. Furthermore, Figure 3 clearly indicates the possibility for strong hysteresis in the operation of the matrix converter.

From a practical perspective, we clearly wish to avoid an oscillatory state in the operation of the matrix converter: a calculation of the linear threshold for the onset of oscillations and the possibility and extent of hysteresis are thus the key relevant results. However, from a mathematical perspective, it is of interest to explore in some more detail the nature of the oscillatory solutions, which we now do.

3.4.1. *Nonlinear development of the oscillatory solution*

One feature of the full numerical solutions presented in Figure 3 is rather puzzling: the branch of stable oscillatory solutions becomes practically impossible to track beyond $V_{or} \approx 40$, because of an escalation in the number of Fourier modes needed to resolve the solution.

To explain this puzzle, we first note that near the Hopf bifurcation point the oscillations in $f_i(t)$ and $g_i(t)$ are very nearly sinusoidal, and are thus well captured by the first few terms in the weakly nonlinear solution of Section 3.3. Similarly, only a few Fourier modes suffice to give a highly accurate numerical solution. However, as we move along the solution branch, the oscillations become less well approximated by a sinusoid, as is illustrated in Figure 4, where we plot the numerical solution for $|f_i(t)|$ and $|g_i(t)|$, on the upper stable branch at $V_{or} = 18.38$. This figure strikingly demonstrates a feature of the oscillatory solution that develops as one moves from the Hopf bifurcation point: evidently $|g_i(t)|$ becomes close to zero at one or more points in the cycle. In view of the requirement to maintain constant output power, $|f_i(t)|$ must correspondingly become large, and there is thus a spike in $|f_i(t)|$. So while $g_i(t)$ does remain *roughly* sinusoidal, $f_i(t)$ has a more complicated time evolution, which leads to the observed rapid increase in Fourier mode truncation N necessary for numerical resolution. Given the practical undesirability of the oscillatory solution, in particular when associated with sharp current spike, as illustrated in Figure 4, we have not attempted to pursue the mathematical question of whether or not the oscillatory solution branch really does cease to exist at some finite value of V_{or}, or whether resolved numerical calculations merely become increasingly hard.

3.5. Analytical approximations for the oscillatory solution

Since it is difficult to make analytical headway with calculation of the oscillatory solution, we now explore two analytical approximations to the oscillatory state, and compare them with our full numerical solution. The first, in Section 3.5.1, is essentially the most naive truncation of the system of equations for the full nonlinear solution. The second, in Section 3.5.2, was originally described by Casadei et al. [2], and turns out (for reasons related to the nonlinear development of the oscillatory solution exemplified in Figure 4) to be a better approximation than the first.

3.5.1. *A drastic truncation*

If we make the most drastic truncation ($N = 1$) of the full nonlinear governing equations for the oscillatory solution, we have

$$f_i^{-1} g_i^{-1*} + f_i^0 g_i^{0*} + f_i^1 g_i^{1*} = \tfrac{2}{3} P_o, \tag{48}$$

$$f_i^0 g_i^{-1*} + f_i^1 g_i^{0*} = 0, \tag{49}$$

$$f_i^{-1} g_i^{0*} + f_i^0 g_i^{1*} = 0, \tag{50}$$

$$Z_i(\omega_i) f_i^0 + g_i^0 = V_{eq}, \tag{51}$$

$$Z_i(\omega_i + \omega_r) f_i^1 + g_i^1 = 0, \tag{52}$$

$$Z_i(\omega_i - \omega_r) f_i^{-1} + g_i^{-1} = 0, \tag{53}$$

with the additional constraint (25) to fix the phases of the Fourier mode amplitudes (of course, an alternative constraint may be substituted for (25), without substantially altering our conclusions, provided it fixes the phase of the solution). Note that in (48)–(53) the superscripts ± 1 and 0 indicate mode numbers (not powers). It thus follows from (49), (50), (52) and (53) that

$$Z_i(\omega_i + \omega_r) Z_i^*(\omega_i - \omega_r) = \left| \frac{g_i^0}{f_i^0} \right|^2 .$$

The oscillation frequency is therefore such that [2]

$$\Im(Z_i(\omega_i + \omega_r) Z_i^*(\omega_i - \omega_r)) = 0.$$

This equation for ω_r is readily solved numerically, for the parameter values in Table I, and gives $\omega_r \approx 10373.5$, which agrees with the result of the linear stability calculation and with the frequency at onset obtained from our full numerical solutions. Notably, in this truncation the frequency of the oscillatory solution is independent of its amplitude: this is not true of the weakly nonlinear solution, nor of the full nonlinear solution.

To solve the remaining equations, we write

$$Z_i(\omega_i + \omega_r) = C_1 \mathrm{e}^{\mathrm{i}\theta}, \qquad Z_i(\omega_i - \omega_r) = C_{-1} \mathrm{e}^{\mathrm{i}\theta}, \tag{54}$$

where $C_{\pm 1}$ are real constants, and introduce the quantity

$$p = \frac{g_i^1 g_i^{-1}}{g_i^{02}}. \tag{55}$$

We emphasise that $C_{\pm 1}$ and θ are *known* quantities. Then (49) and (50) become

$$f_i^1 = -\frac{f_i^0 g_i^{-1*}}{g_i^{0*}} = -\frac{f_i^0 g_i^{0*} p^*}{g_i^{1*}}, \qquad f_i^{-1} = -\frac{f_i^0 g_i^{1*}}{g_i^{0*}} = -\frac{f_i^0 g_i^{0*} p^*}{g_i^{-1*}}. \tag{56}$$

From (52), (53), (54) and (56), it follows that

$$C_1 \mathrm{e}^{\mathrm{i}\theta} f_i^0 g_i^{0*} p^* = |g_i^1|^2, \qquad C_{-1} \mathrm{e}^{\mathrm{i}\theta} f_i^0 g_i^{0*} p^* = |g_i^{-1}|^2. \tag{57}$$

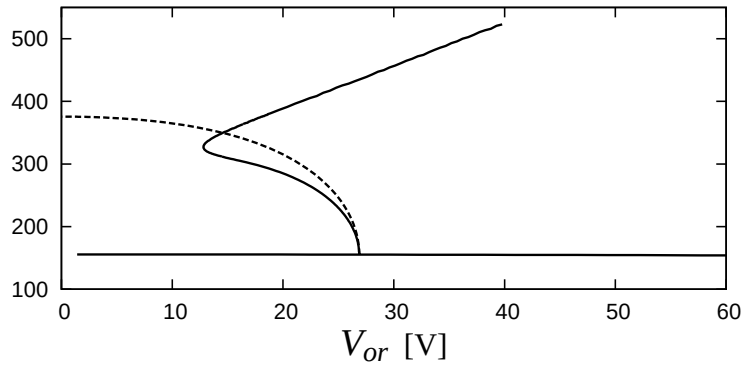

Figure 5. Solutions to (46) and (47) truncated at $N = 1$ (dashed line). Plotted vertically is, for the steady state, $\Re(g_i)$, and for the oscillatory solution the maximum value of $\Re(g_i(t))$ over the cycle. The solid lines show all the fully resolved solution branches of Figure 3, without truncation (thus one should not infer *stability* of these solutions from the type of line used in this plot — see Figure 3 for stability information).

These expressions motivate us to introduce the *real* parameter μ such that

$$\mathrm{e}^{\mathrm{i}\theta} f_i^0 g_i^{0*} p^* = \tfrac{2}{3}\mu P_o; \tag{58}$$

then $|g_i^{\pm 1}|^2$ are given parametrically in terms of μ by

$$|g_i^1|^2 = \tfrac{2}{3}\mu P_o C_1, \qquad |g_i^{-1}|^2 = \tfrac{2}{3}\mu P_o C_{-1}. \tag{59}$$

Furthermore, from (48) and (56) we see that

$$f_i^0 g_i^{0*} = \tfrac{2}{3} P_o (1 - 2p^*)^{-1}; \tag{60}$$

hence p is determined parametrically in terms of μ by

$$p = \frac{\mu}{\mathrm{e}^{-\mathrm{i}\theta} + 2\mu}, \tag{61}$$

in view of (58) and (60). Now from (55) and (59) we see that we may write

$$|g_i^1| = |g_i^0||p|^{1/2}(C_1/C_{-1})^{1/4}, \qquad |g_i^{-1}| = |g_i^0||p|^{1/2}(C_{-1}/C_1)^{1/4}. \tag{62}$$

It now follows from (59) and (62) that the output power is

$$P_o = \frac{3|p||g_i^0|^2}{2\mu(C_1 C_{-1})^{1/2}}. \tag{63}$$

Finally, from (51) we obtain the single equation to determine g_i^0 parametrically in terms of μ:

$$\left(\frac{Z_i(\omega_i)|p|}{\mu(C_1 C_{-1})^{1/2}(1 - 2p^*)} + 1 \right) g_i^0 = V_{eq} \tag{64}$$

or, more explicitly,

$$\left(\frac{Z_i(\omega_i)|\mu|(1 + 2\mu\mathrm{e}^{-\mathrm{i}\theta})}{(C_1 C_{-1})^{1/2}\mu|\mathrm{e}^{-\mathrm{i}\theta} + 2\mu|} + 1 \right) g_i^0 = V_{eq}. \tag{65}$$

We now see how the truncated solution is obtained. We first use (65) to give g_i^0 parametrically in terms of the real parameter μ. Once g_i^0 has been obtained, the values of $|g_i^1|$ and $|g_i^{-1}|$ may be found

from (62). Since p is given by (61), the *sum* of the arguments of g_i^1 and g_i^{-1} is known from (55); their individual arguments then follow from the constraint (25). Now the output power is given parametrically in terms of μ from (63). Once P_o is found, f_i^0 may be found from, for example, (60). Then f_i^1 and f_i^{-1} follow from (56). This completes the specification of the solution.

Figure 5 compares this truncated solution with the full numerical solution. Agreement is excellent near the bifurcation point, but significantly worsens further away. Most significantly, the severely truncated solution branch does not have a turning point (saddle–node bifurcation), and so fails to describe the stable oscillatory solution. The reason for the increasingly poor agreement is that this truncation assumes that both $f_i(t)$ and $g_i(t)$ remain close to sinusoidal all along the oscillatory solution branch (which Figure 4 shows is not the case). One might try to improve this approximation by adding a few more harmonics to the truncation (by increasing N from 1 to, say, 2 or 3 or 4), but this yields an approximation that turns out to be little better than the $N = 1$ truncation described above. We therefore turn next to an alternative approximation.

3.5.2. *A better approximation*

Casadei et al. [2] provide an alternative means of calculating an approximate oscillatory state. Although their truncation seems at first sight similar to that of the section above, it turns out to be rather better, for reasons that we shall explain below. We now give a slightly adapted description of their method. As in the previous section, the input voltage and current in the oscillatory state are approximated using the first terms in their Fourier expansion, so that

$$f_i = f_i^0 + f_i^1 \mathrm{e}^{\mathrm{i}\omega_r t} + f_i^{-1} \mathrm{e}^{-\mathrm{i}\omega_r t}, \tag{66}$$

$$g_i = g_i^0 + g_i^1 \mathrm{e}^{\mathrm{i}\omega_r t} + g_i^{-1} \mathrm{e}^{-\mathrm{i}\omega_r t}. \tag{67}$$

But now, instead of using (48)–(50), the means of calculating the various coefficients in (66) and (67) is to *suppose that g_i is given exactly by (67)*, and to compute the corresponding full Fourier series for f_i, using

$$f_i = \tfrac{2}{3} P_o / g_i^*,$$

which follows from (28). Finally, this Fourier series for f_i is truncated to give (66). Thus we have

$$f_i^0 = \frac{1}{2\pi} \int_0^{2\pi} \frac{\frac{2}{3}P_o}{g_i^{0*} + g_i^{1*}\mathrm{e}^{-\mathrm{i}t} + g_i^{-1*}\mathrm{e}^{\mathrm{i}t}} \,\mathrm{d}t = \frac{\frac{2}{3}P_o}{g_i^{0*}\delta}, \tag{68}$$

$$f_i^1 = \frac{1}{2\pi} \int_0^{2\pi} \frac{\frac{2}{3}P_o \mathrm{e}^{-\mathrm{i}t}}{g_i^{0*} + g_i^{1*}\mathrm{e}^{-\mathrm{i}t} + g_i^{-1*}\mathrm{e}^{\mathrm{i}t}} \,\mathrm{d}t = \frac{\frac{1}{3}P_o}{g_i^{1*}} \left(1 - \delta^{-1}\right), \tag{69}$$

$$f_i^{-1} = \frac{1}{2\pi} \int_0^{2\pi} \frac{\frac{2}{3}P_o \mathrm{e}^{\mathrm{i}t}}{g_i^{0*} + g_i^{1*}\mathrm{e}^{-\mathrm{i}t} + g_i^{-1*}\mathrm{e}^{\mathrm{i}t}} \,\mathrm{d}t = \frac{\frac{1}{3}P_o}{g_i^{-1*}} \left(1 - \delta^{-1}\right), \tag{70}$$

where

$$\delta = \left(1 - \frac{4 g_i^{1*} g_i^{-1*}}{g_i^{0*2}}\right)^{1/2}, \tag{71}$$

and the square root is chosen so that the real part of δ lies in the right-hand half of the complex plane. The specification of the problem is completed by (51)–(53) and (25).

A consideration of Figure 4 shows why it is desirable to choose g_i to be given by (67) and then to truncate a full Fourier expansion of f_i, rather than the other way round. This is because g_i remains roughly sinusoidal along the oscillatory solution branch, even while f_i has significantly more complicated time evolution. (A similar calculation, but with f_i assumed to be given exactly by (66), and with the coefficients in (67) then given by expressions analogous to (68)–(70), but with the roles of f_i and g_i interchanged, yields significantly worse results, although these are not reported here.)

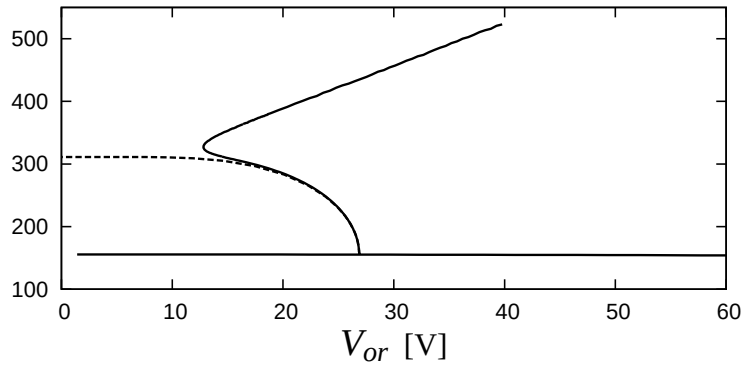

Figure 6. Solutions to the Casadei et al. [2] approximation (68)–(70) (dashed line). Plotted vertically is, for the steady state, $\Re(g_i)$, and for the oscillatory solution the maximum value of $\Re(g_i(t))$ over the cycle. The solid lines show all the fully resolved solution branches of Figure 3, without truncation (thus, as in Figure 5, one should not infer *stability* of these solutions from the type of line used in this plot — see Figure 3 for stability information).

Now that we have the relationships (68)–(70) between the components of f_i and those of g_i, we may follow a procedure similar to that described in the previous section to obtain the solution (this is the procedure followed by Casadei et al. [2]). Writing $Z_i(\omega_i \pm \omega_r)$ in the form (54), and defining p as in (55), we see from (52) and (53) that

$$Z_i(\omega_i + \omega_r)\frac{P_o}{3|g_i^1|^2}\left(1-\delta^{-1}\right) = Z_i(\omega_i - \omega_r)\frac{P_o}{3|g_i^{-1}|^2}\left(1-\delta^{-1}\right) = -1. \tag{72}$$

Thus, introducing the real parameter

$$\lambda = \frac{3|g_i^1|^2}{C_1 P_o}, \tag{73}$$

we have, from (72),

$$\delta = \frac{1}{1+\lambda \mathrm{e}^{-\mathrm{i}\theta}} \tag{74}$$

and hence, using (55) and (71), we have

$$p = \tfrac{1}{4}(1-(1+\lambda \mathrm{e}^{\mathrm{i}\theta})^{-2}). \tag{75}$$

Now we note that from (72),

$$C_1|g_i^{-1}|^2 = C_2|g_i^1|^2,$$

and hence the harmonics of g_i are related to the fundamental by

$$|g_i^1| = |g_i^0||p|^{1/2}(C_1/C_{-1})^{1/4}, \qquad |g_i^{-1}| = |g_i^0||p|^{1/2}(C_{-1}/C_1)^{1/4} \tag{76}$$

(these expressions are the same as in the truncated case of the previous section). Thus from (73) and (76) the power is given by

$$P_o = \frac{3|g_i^0|^2|p|}{\lambda(C_1C_{-1})^{1/2}}. \tag{77}$$

Finally, the parametric equation for the fundamental (in terms of λ) is

$$\left(\frac{2Z_i(\omega_i)|p|(1+\lambda \mathrm{e}^{-\mathrm{i}\theta})}{\lambda(C_1C_{-1})^{1/2}} + 1\right) g_i^0 = V_{eq}. \tag{78}$$

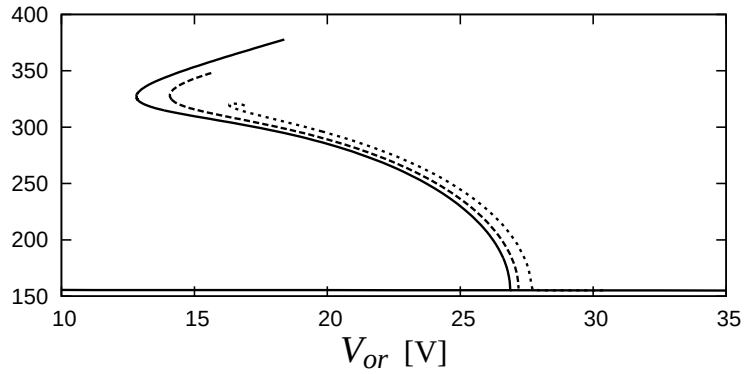

Figure 7. Solutions to the nonlinear system (4)–(11) with delay $T = 0$ (solid line), $T = 4\text{e}{-6}$ (dashed line) and $T = 10\text{e}{-6}$ (dotted line) as a function of the output reference voltage V_{or}. (Again, we stress that one should not infer *stability* of these solutions from the type of line used in this plot.) Both sets of results are obtained using the Fourier-series approach. Plotted vertically is, for the steady state, $\Re(g_i)$, and for the oscillatory solution the maximum value of $\Re(g_i(t))$ over the cycle. The oscillatory branches terminate when the numerical procedure requires too many Fourier modes to continue.

Figure 6 compares the approximate solution derived above with the full numerical solution. As for the truncated solution described in the previous section, agreement is excellent near the bifurcation point. Furthermore, the present approximation remains closer to the branch of unstable oscillatory solutions than the drastic truncation of the previous section (compare Figures 5 and 6). Unfortunately, both approximations lack the turning point, and so fail to capture either the stable oscillatory solutions or the possibility of hysteresis; for these, we need the fully nonlinear numerical solutions.

It is worth noting that Casadei et al. [2] determined mathematical expressions for this approximate solution, but did not discuss its specific dependence on the parameters of the problem. As a consequence, they were unable to conclude that the associated bifurcation to the oscillatory state is *subcritical*, which our presentation makes clear. Neither did they emphasise, as we are able to do on the basis of our comparison with the fully nonlinear solution, that their approximation represents an *unstable* solution. Finally, our presentation makes clear that the Casadei et al. approximation does not capture the saddle–node bifurcation at which a stable oscillatory state emerges.

4. Results for nonzero delay

In this section we briefly describe calculations of the oscillatory solutions for a variety of nonzero delay times. To do so, we start from the zero-delay solutions described above and continue them in a delay time parameter T. We have used only our Fourier-series method for the delay case, because AUTO is not presently suited to such problems. The results for nonzero delay are qualitatively similar to those for $T = 0$.

In the presence of delays, (10) and (11) are replaced by

$$\hat{m}_d(\omega) = D(\omega, T)\hat{m}_{dr}(\omega), \qquad \hat{m}_i(\omega) = D(\omega, T)\hat{m}_{ir}(\omega),$$

where the relevant delay operator is [2, 3]

$$D(\omega, T) = \frac{(1 - \mathrm{e}^{-\mathrm{i}\omega T})\mathrm{e}^{-\mathrm{i}\omega T}}{\mathrm{i}\omega T}, \tag{79}$$

and T is a delay time constant, typically the period of the high-frequency switching in the matrix converter; for example, $T = 80\mu$s when the switching takes place at 12.5kHz. Note that in the limit

$T \to 0$, we recover the zero-delay model, since in that limit, from (79), we take

$$D(\omega, 0) = \lim_{T \to 0} D(\omega, T) = 1.$$

For $T = 4\text{e}{-6}$, and $T = 10\text{e}{-6}$ (seconds) the solution branches are illustrated in Figure 7, and compared with those for $T = 0$. We note that the introduction of a delay tends to stabilise the matrix converter: both the linear threshold for instability and the saddle–node turning point move to increased values of V_{or} as T is increased. We find that, as in the case of no delays, the solution for $g_i(t)$ remains reasonably well approximated as sinusoidal close to the bifurcation point, but again a spike develops in $f_i(t)$ as we traverse the solution branch. As the delay parameter T is increased, the point at which the branch effectively terminates (due to a need for excessively many Fourier modes to allow adequate resolution of this spike) occurs earlier. Indeed, we have found it practically impossible to continue the oscillatory solution branch much beyond $T = 10\text{e}{-6}$. In particular we have been unable to reach $T = 80\text{e}{-6}$, which corresponds to typical operating conditions for the matrix converter, although it is not clear whether this is the result of the mathematical solution ceasing to exist or simply insurmountable numerical difficulties in trying to achieve convergence.

5. Numerical simulations of the matrix converter

For the case of zero delay ($T = 0$), we have carried out two sorts of direct numerical simulations of the matrix converter system. First, we have used the Saber® simulator [10]. Saber is an electrical circuit orientated simulator which allows the entire matrix converter system, excluding the converter, to be modelled directly using supplied library elements. A functional representation is used for the converter, in which switching elements are replaced by continuous current and voltage sources representing the modulating functions (time averaged duty cycles) of each switch [11, 12]. Modulation calculations, using the Venturini algorithm [13, 14, 15], are implemented using the Mast® programming language of Saber. The standard Saber second-order Gear time-stepping algorithm is employed with a 200ns fixed time-step. All other simulation control parameters are set to the default values. The initial condition is a small perturbation from the steady-state solution.

Typical results of the Saber simulations are shown in Figure 8, at $V_{o,r} = 28\text{V}$ (just above the linear instability threshold $V_{o,rc} \approx 26.88\text{V}$ computed above). Here, the theory predicts that the steady-state solution is unstable, and that the stable solution is the oscillatory state with large-amplitude ripple (see, for example, Figure 3). The rapid growth of high-frequency ripple is clearly evident on (for example) the input voltage $v_i^{(1)}$, shown in Figure 8(a). A fast Fourier transform of a section of the signal shows that the ripple has a frequency of approximately 1650Hz (which agrees well with the linear prediction of 1651Hz). The plot of $|g_i(t)|$ in Figure 8(b) effectively factors out the 50Hz oscillation of the input voltages, and the catastrophic growth of the ripple is more clearly evident. The simulations break down at $t \approx 0.061$, at which point $g_i(t)$ is close to zero. Thus, although a stable oscillatory solution exists for these parameter values, the numerical simulation does not approach it from the given initial condition: presumably the chosen initial condition is not in the basin of attraction of the oscillatory state (or, if it *is*, then integration tolerances need to be improved to see the approach to the oscillatory state). It is possible that the oscillatory state could be found, either by improving integration tolerances in the Saber simulations or by choosing an different initial condition. However, the oscillatory state involves such extreme oscillations that it is highly undesirable for practical engineering purposes, so we have not tried further to find it. Nevertheless, we note that the large amplitude of the ripples seen in the simulation is qualitatively consistent with the theoretically predicted subcritical nature of the bifurcation to oscillations. Further, the breakdown of the solution when $g_i(t)$ gets close to zero is consistent with the numerical termination of the oscillatory solution branches found above (see, for example, Figure 3).

We have also simulated the ODE model (38) using `dsolve` in the computer algebra package Maple. Our results are consistent with those described above: for instance, we find excellent agreement about

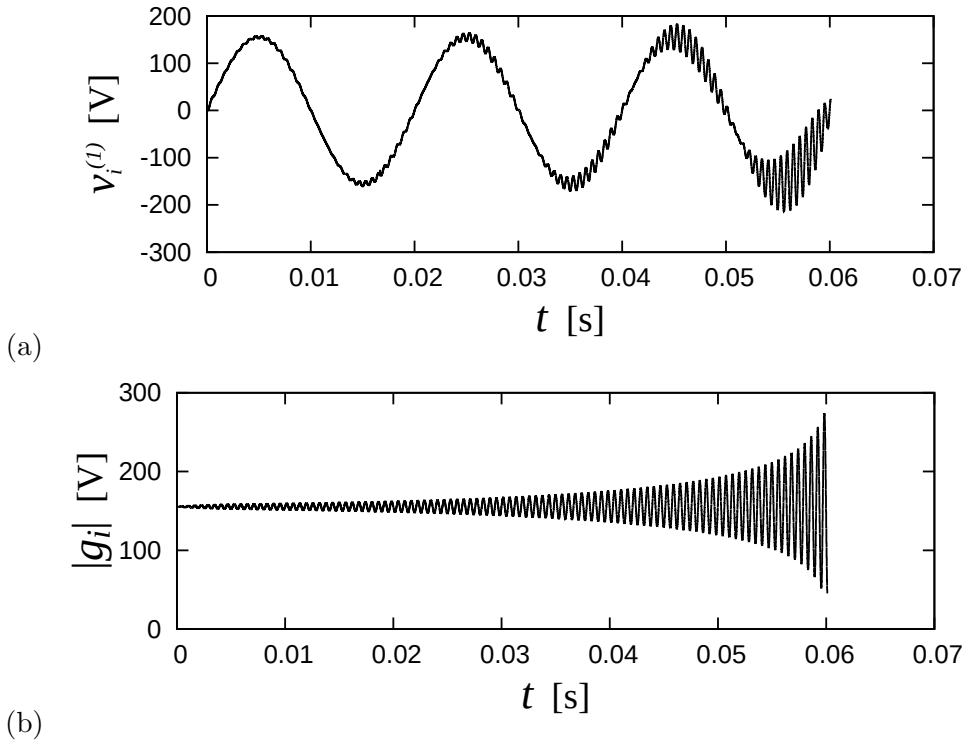

Figure 8. Saber® simulations at $V_{o,r} = 28$V. (a) Plot of $v_i^{(1)}(t)$: note the growth of large-amplitude ripple on the nominally 50Hz voltage. (b) Plot of $|g_i(t)|$, showing the growth of oscillations in the input voltage space vector. Simulations are unable to continue beyond $t \approx 0.061$, when $|g_i(t)|$ appears to hit zero.

the point at which the steady state becomes unstable and about the frequency of small-amplitude ripple. Furthermore, we find that the oscillatory state has a very small basin of attraction, so that simulations must be started exceedingly close to that state and integration tolerances must be carefully chosen for the oscillatory state to be observed (38).

We close this section by noting one manifestation of the saddle–node point that is apparent in our Maple simulations. We take V_{or} just *below* the saddle–note point, and vary the initial condition for our simulations: in this example we happen to vary $F \equiv f_i(0)$ (which, through (37), determines $g_i(0)$), with the remaining initial conditions given by $\dot{g}_i(0) = \ddot{g}_i(0) = 0$, although other choices yield similar results. We find a threshold behaviour as F (which we take to be real and non-negative) is varied. For example, when F is sufficiently small, the solution ultimately tends to the steady state; by contrast, for larger values of F, we find that the solution blows up after a few oscillations. These oscillations are the vestiges of the oscillatory solution, which of course no longer exists below the saddle–node point. We illustrate this behaviour in Figure 9.

6. Conclusion and discussion

We have extended the model of Casadei et al. [2, 3], which describes the stability of a matrix converter, to the fully nonlinear regime. For the parameters used by Casadei et al. [3], we have shown, through a weakly nonlinear analysis and complementary direct numerical solution of the full nonlinear governing equations, that the instability of the steady-state operating condition is a *subcritical* Hopf bifurcation. The unstable branch of oscillatory solutions then undergoes a saddle–node bifurcation, at which it becomes stable. This bifurcation scenario has two practically significant consequences. First, it means

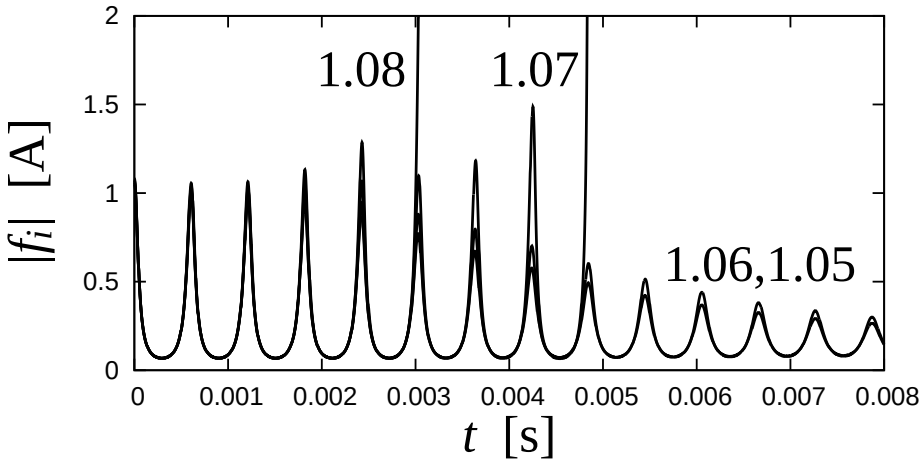

Figure 9. Plot of $|f_i(t)|$ according to simulations of (38) using `dsolve` in Maple, at $V_{or} = 12.81$, just below the saddle–node point. In each case the initial value for f_i is indicated next to the relevant curve (correspondingly $g_i(0) = \frac{2}{3}P_o/f_i^*$, according to (37)); in addition we set $\dot{g}_i(0) = 0$ and $\ddot{g}_i(0) = 0$. For $f_i = 1.07$ or 1.08 (or greater), the solution oscillates then blows up. For $f_i = 1.05$ or 1.06 (or less) the solution tends, after significant oscillations, to the steady state.

that stable oscillatory solutions exist well below the threshold value of V_{or} available from (the rather simpler) linear theory. Second, it indicates that solutions are subject to strong hysteresis as V_{or} is varied. It is particularly significant that the converter is thus rather *more* susceptible to oscillations than the linear theory would suggest.

Another significant feature of our results for future model development is that (whether or not the effects of delay are included in the analysis) the oscillatory solution develops a spike in the input current. The presence of the spike manifests itself in a need to take an increasing number of Fourier modes in our numerical scheme to resolve the oscillations as one moves along the branch; eventually it becomes practically impossible to continue tracking the solution branch. As well as being practically highly undesirable, the presence of a spike calls into question the underlying modelling assumption that the high-frequency switching of the device may be discounted in analysis of its stability. This is because, while the oscillatory solution itself has a period significantly in excess of the switching period of the matrix converter, the spike evolves over a much shorter time scale, which may in fact be comparable with the switching period. Our results suggest that a proper analysis of matrix converter stability should include switching effects. (It may instead be that some other feature of a real matrix converter, which is not included in the model of Casadei et al. [2, 3], suppresses the spiking, so that continued neglect of the high-frequency switching is in fact justified.) There is a vast literature examining the effects of switching, on a wide variety of electronic devices [4], including different types of power converter, primarily DC–DC [7]. Not only can the "slow-scale" instability such as examined here be quantitatively modified by the finite switching frequency, but other, new, "fast-scale" instabilities can arise [4, 5, 6, 7, 16]. Indeed, on the mathematical side, the analysis of piecewise-smooth dynamical systems is a vast area of research in its own right (see, for example the recent work of di Bernardo et al. [17]).

Finally, it may also be worthy of note that our Fourier ansatz for the oscillatory solution allows only solutions for which the variables in (15) are singly periodic functions of time. Any further bifurcations from the oscillatory branch, leading to either quasiperiodic or chaotic solutions, could not be captured with the Fourier ansatz assumed here.

Acknowledgements

This work was supported by the Engineering and Physical Sciences Research Council [grant number EP/E018580/1].

References

1. Wheeler PW, Rodríguez J, Clare JC, Empringham L, Weinstein A (2002) Matrix converters: a technology review. IEEE Trans Industr Electr 49:276–288.
2. Casadei D, Clare J, Empringham L, Serra G, Tani A, Trentin A, Wheeler P, Zarri L (2007) Large-signal model for the stability analysis of matrix converters. IEEE Trans Industr Electr 54:939–950.
3. Casadei D, Serra G, Tani A, Trentin A, Zarri L (2005) Theoretical and experimental investigation on the stability of matrix converters. IEEE Trans Industr Electr 52:1409–1419.
4. Banerjee S, Verghese GC (2001) Nonlinear phenomena in power electronics: bifurcations, chaos, control and applications. Wiley-IEEE Press.
5. Mazumder SK, Nayfeh AH, Boroyevich D (2001) Theoretical and experimental investigation of the fast- and slow-scale instabilities of a DC–DC converter. IEEE Trans Power Electr 16:201–216.
6. Mazumder SK, Nayfeh AH, Boroyevich D (2003) An investigation into the fast- and slow-scale instabilities single phase bidirectional boost converter. IEEE Trans Power Electr 18:1063–1069.
7. Tse CK (2003) Complex behavior of switching power converters. CRC Press, Boca Raton.
8. Cox SM, Creagh SC (2009) Voltage and current spectra for matrix power converters. SIAM J Appl Math 69:1415–1437. http://dx.doi.org/10.1137/080718863
9. Casadei D, Serra G, Tani A, Zarri L (2002) Matrix converter modulation strategies: a new general approach based on space-vector representation of the switch state. IEEE Trans Industr Electr 49:370–381.
10. Saber. `http://www.synopsys.com/products/mixedsignal/saber/saber.html`.
11. Clare JC, Wheeler PW, Empringham L (2003) Modelling and design of matrix converter solutions for shipboard applications. IMarEST Electric Warship Seminar, December 2003.
12. Zanchetta P, Clare JC, Wheeler PW (2003) CAD of matrix converter systems and their control for AC power supplies. In: European Power Electronics Conference, Toulouse, 2003.
13. Alesina A, Venturini M (1981) Solid-state power conversion: a Fourier analysis approach to generalized transformer synthesis. IEEE Trans Circuits and Systems 28:319–330.
14. Venturini M (1980) A new sine wave in, sine wave out conversion technique eliminates reactive elements. In: Proceedings of the National Solid State Power Conversion Conference, San Diego (Powercon7), 1980, E3_1–E3_15.
15. Venturini M, Alesina A (1980) The generalised transformer: a new bidirectional sinusoidal waveform frequency converter with continuously adjustable input power factor. In: Proceedings of the IEEE Power Electronics Specialists Conference, 1980, 242–252.
16. Fossas E, Olivar G (1996) Study of chaos in the buck converter. IEEE Trans Circuits and Systems I 43:13–25.
17. di Bernardo M, Budd CJ, Champneys AR, Kowalczyk P (2008) Piecewise-smooth dynamical systems: theory and applications. Springer, London.